Materials Science and Engineering A 528 (2011) 1787–1798

Contents lists available at ScienceDirect

Materials Science and Engineering A

journal homepage: www.elsevier.com/locate/msea

Effect of mushy state rolling on age-hardening and tensile behavior of Al–4.5Cu alloy and in situ Al–4.5Cu–5TiB_2 composite

I.G. Siddhalingeshwar[a], M.A. Herbert[b], M. Chakraborty[c], R. Mitra[a,*]

[a] Department of Metallurgical and Materials Engineering Indian Institute of Technology, Kharagpur 721302, West Bengal, India
[b] Department of Mechanical Engineering, National Institute of Technology, Surathkal 575025, Karnataka, India
[c] Indian Institute of Technology, Bhubaneswar 751013, Orissa, India

ARTICLE INFO

Article history:
Received 21 July 2010
Received in revised form 4 November 2010
Accepted 5 November 2010

Keywords:
B. Aluminum alloys
Composites
C. Semisolid processing
Bulk deformation
D. Age hardening
Precipitation

ABSTRACT

The effect of mushy state rolling on aging kinetics of stir-cast Al–4.5Cu alloy and in situ Al–4.5Cu–5TiB_2 composite and their tensile behavior in solution-treated (495 °C) or differently aged (170 °C) conditions, has been investigated. As-cast or pre-hot rolled alloy and composite samples were subjected to single or multiple mushy state roll passes to 5% thickness reduction at temperatures for 20% liquid content. Peak-aging times of mushy state rolled composite matrices have been found as ≈7.5–10% of that of as-cast alloy. Such enhancement in aging kinetics is attributed to homogeneity in Cu atom distribution as well as increase in matrix dislocation density due to thermal expansion coefficient mismatch between Al and TiB_2, matrix grain refinement and particle redistribution, achieved by mushy state rolling. Uniform precipitate distribution in mushy state rolled composite matrices leads to greater peak-age microhardness with higher yield and ultimate tensile strengths than those in as-cast alloy and composite.

1. Introduction

In recent years, there has been a great deal of interest in discontinuously reinforced aluminum alloy matrix composites (DRA) due to their attractive properties, such as low density, high specific modulus, high specific strength, isotropic character and relative ease of fabrication. These properties are responsible for worldwide interest in development of suitable DRA composites for a variety of automotive, military and aerospace applications [1–3]. The interest in heat treatment of the age-hardenable Al alloy matrix of DRA composites arises from their enhanced aging kinetics with respect to those of the corresponding unreinforced Al alloys, as reported in the literature [4–16]. The accelerated age-hardening of the composite matrices has been attributed to the presence of higher density of dislocations than that in the unreinforced Al alloy. It has been reported [17,18] with adequate evidence that dislocations are punched out at the reinforcement–matrix interfaces to relax the stresses generated owing to mismatch in their coefficients of thermal expansion (CTE). It is also well-known that prior tensile stretching of the solution treated Al alloys leads to enhanced and more homogeneous precipitation, as the dislocation density is increased.

Mushy state processing of as-cast commercial alloys and metal–matrix composites by thixo-forming and thixo-extrusion has received significant attention in recent years [19,20], as these processing routes require considerably smaller flow stress than that for conventional working methods [21,22]. It has been reported [23] that the microstructures of the Al alloys processed by semi-solid processing show a refined equiaxed grain structure formed by the nucleation and growth of spheroidal grains during recrystallization in the semi-solid state. Recently, it has been reported [24] that mushy state rolling of cast Al–4.5Cu–5 wt.% TiB_2 composite at temperatures corresponding to 10–30 vol.% liquid, leads to refinement of rosette-shaped grain structure in the α-Al matrix of the as-cast composite to form globular or equiaxed grains. Moreover, both wear and mechanical properties of this composite have been found to improve significantly on mushy state rolling, due to chemical homogenization, grain refinement, and limited work hardening of the unmelted matrix grains due to deformation [25,26]. Work hardening of the matrix is also expected due to the creation of dislocations to accommodate the mismatch in CTE between the Al matrix and ceramic reinforcement during cooling from the temperature of semi-solid processing [17,18].

So far, limited information is available on aging behavior of the Al–Cu alloys and their composites processed by semisolid processing in general, and mushy state rolling in particular. The present study is an attempt to examine the effect of mushy sate rolling and number of roll passes on the aging kinetics of the matrix of in situ

* Corresponding author. Tel.: +91 3222 283292; fax: +91 3222 282280.
E-mail address: rahul@metal.iitkgp.ernet.in (R. Mitra).

0921-5093/$ – see front matter © 2010 Elsevier B.V. All rights reserved.
doi:10.1016/j.msea.2010.11.027

Al–4.5 wt.% Cu–5 wt.% TiB_2 composite, and is accompanied by a thorough analysis of the scientific causes for the observed behavior. Moreover, the effect of solutionizing and aging heat-treatments on tensile behavior of the as-cast alloy, as-cast composite and mushy state rolled composite has also been evaluated.

2. Experimental procedure

2.1. Processing

First, a master alloy with composition of Al–33 wt.% Cu was prepared in an induction melting furnace. Thereafter, the Al–4.5Cu alloy (referred to as "alloy" in the text) was prepared from the master alloy by adding suitable amount of Al. In situ Al–4.5Cu–5TiB_2 composite (referred to as "composite" in the text) was processed through stir casting method, in which the TiB_2 particles were precipitated in situ by a mixed salt route. The method used for processing of both alloy and composite, has been reported in detail elsewhere [9,24].

2.2. Mushy state rolling

A two-high rolling mill with rolls of 120 mm diameter and 125 mm barrel width, was used for the mushy state rolling experiments. Prior to mushy state rolling, the composite specimens were subjected to hot rolling for 2.5% reduction in thickness at 370 °C, for both partial homogenization and avoiding of alligatoring during mushy state rolling of these materials [21]. Both alloy and composite specimens with dimensions of 40 mm × 25 mm × 6 mm were subjected to mushy state rolling for 5% thickness reduction at 625 and 626 °C (temperature for 20 vol.% liquid), respectively at a constant roll surface velocity of 0.28 ms^{-1}. Samples of the investigated composite were also subjected to multiple (2 or 3) mushy state roll passes at 626 °C, with 5% reduction in thickness per pass. The procedure used for mushy state rolling has been explained in detail in an earlier report [24]. Presence of 20 vol.% of liquid in the investigated alloy and composite samples at the soaking temperature was confirmed prior to mushy state rolling, following a procedure described in detail elsewhere [24,27]. Later in this manuscript, the as-cast or mushy state rolled alloy has been referred to ACA or MRA, respectively, while the abbreviations used for as-cast, hot rolled, or mushy state rolled (single pass) composites are ACC, HRC or MRC, respectively. Furthermore, the composites subjected to one, two and three mushy state roll passes after prior hot rolling have been named as PHMPR1, PHMPR2 and PHMPR3, respectively.

2.3. Solutionizing and aging treatments with microhardness measurements

The samples of alloy and composite, in as-cast condition as well as after mushy state rolling were subjected to age-hardening heat-treatments. The experimental conditions for aging were chosen, following the procedure recommended in the ASTM standards [28]. A muffle furnace with an accuracy limit of ±3 °C was used to carry out the heat-treatments. The cycles of heat treatment included solutionizing at 495 °C for 2 h, followed by aging at 170 °C for different periods of time. After the completion of soaking for solution-treatment, the samples were quenched in an ice-cold water bath, keeping the time for transfer as minimum. During aging, the samples were taken out of the furnace at different time intervals and air-cooled to room temperature. Microhardness measurements were carried out on either solution-treated or differently aged specimens in metallographically polished conditions, using a Vickers microhardness tester (model: MICROMET 5103, Buehler Ltd., IL, USA) operated at a load of 100 gf.

2.4. Microstructural characterization

Microstructures of both the alloy and the composite in either as-cast or mushy state rolled conditions were investigated using optical microscopy as well as secondary (SE) and back scattered electron (BSE) imaging on a field emission scanning electron microscope (FESEM-Model: Zeiss Supra 40; Carl Zeiss SMT, Germany), equipped with an energy dispersive spectrometer (EDS, Oxford Instruments, Abingdon, Oxfordshire, UK). Furthermore, the phases present in solution treated or peak aged alloys or alloy matrices of the investigated composites were identified by X-ray diffraction (XRD). In addition, electron transparent specimens for transmission electron microscopy studies were prepared by mechanical thinning, followed by thinning on a dimple grinder (Gatan, CA, USA) to reduce their thickness to 20 μm; and finally argon ion thinning on a precision ion polishing system (PIPS Model: 691, Gatan, CA, USA). Subsequently, these specimens were examined using bright and dark field imaging modes on a transmission electron microscope (TEM, Model: JEM 2100, JEOL, Japan) operated at an acceleration voltage of 200 kV, and digital images were recorded.

2.5. Tensile testing

Tensile tests were carried out at a nominal strain rate of $3.125 \times 10^{-4}\ s^{-1}$ on a universal testing machine (model: Instron 3365, INSTRON Ltd., UK), in which the elongation was measured using a static axial clip-on extensometer (model: Instron, Strain gauge type, 2630-102). These tests were carried out on flat specimens with gage length of 16 mm and cross-section of 4 mm × 4 mm, machined following the ASTM standard E-8M, from the plates of ACA, ACC in peak aged condition and MRC in solution-treated, under-aged (0.5 h), peak-aged (2 h), as well as over-aged (4 h) conditions. The fracture surfaces of the tension-tested specimens were examined using FESEM, whereas the chemical compositions at specific locations were investigated by using EDS.

3. Results

3.1. Microstructure

3.1.1. As cast and mushy state rolled condition

Optical micrographs depicting the typical microstructures of as-cast alloy and composite are shown in Fig. 1(a) and (b), respectively, while those of the mushy state rolled alloy and composite samples are shown in Fig. 1(c) and (d), respectively. In addition, an optical micrograph depicting the grain structure in PHMPR2 is shown in Fig. 1(e). The microstructures of as cast alloy and composite samples show typical dendritic and rosette-like irregular grain structure, respectively. Examination of the microstructures of ACA at higher magnification has shown the presence of coarse $CuAl_2$ particles at interdendritic locations, as reported in an earlier study [24]. Furthermore, the microstructure of the MRA [Fig. 1(c)] shows presence of both irregular and equiaxed grains, which appear to be much coarser than those found in the microstructure of the MRC [Fig. 1(d)]. Moreover, comparison of the microstructures of PHMPR2 [Fig. 1(e)] and MRC [Fig. 1(d)] shows apparently finer grain size in the former material.

The mechanisms for evolution of grain structure in the mushy state rolled alloy and composites have been discussed in detail in an earlier report [24]. Both alloy and composite samples have shown bimodal grain size distributions, in which formation of the fine grains is believed to be caused by rapid solidification of liquid, particle stimulated dynamic recrystallization and grain fragmentation in the unmelted solid skeleton, while the presence of large grains has been attributed to coarsening of the unmelted grains.

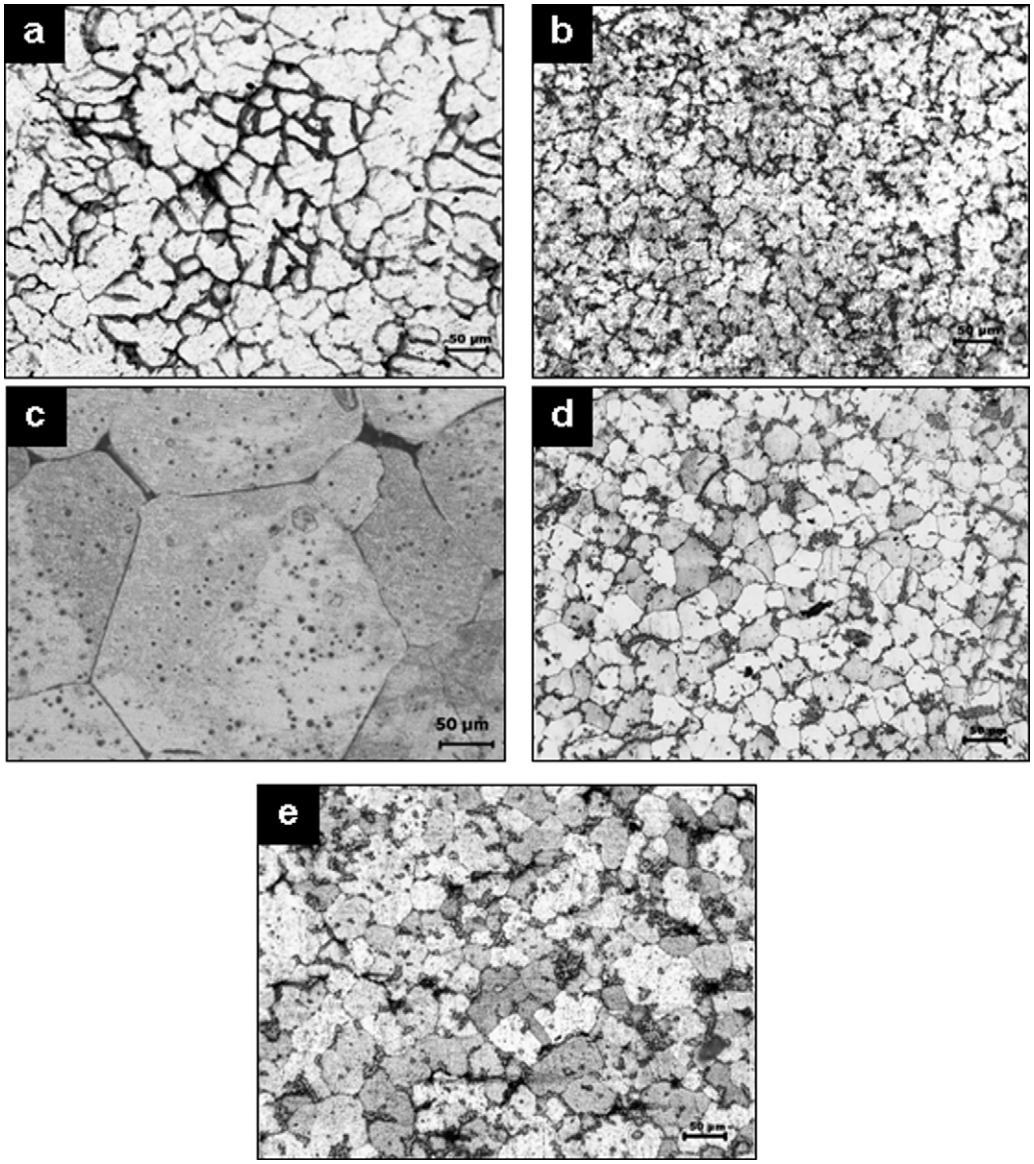

Fig. 1. Optical micrographs showing the microstructures of: (a) ACA, (b) ACC, (c) MRA, (d) MRC, and (e) PHMPR2.

The average aspect ratio (length to diameter) of the areas enclosed within the dendrites of ACA has been found as approximately 4.3:1, while the average size of the rosette-shaped grains of ACC has been found as ~50 μm. The average sizes of coarse and fine grains in all the investigated materials are shown in Table 1. Examination of the results in this table indicates that (i) the average sizes of coarse and fine grains in MRA are much larger than the corresponding sizes in the matrix of MRC, (ii) the grain refinement in PHMPR1 is more significant than that found in case of HRC or MRC; and (iii) the coarse grains undergo much greater reduction in their average size than the fine grains with increase in the number of mushy state roll passes after prior hot rolling. The first observation is attributed to the role of grain boundary pinning by the TiB_2 particles in the composite. The second inference suggests that compositional homogenization and strain induced by prior hot rolling triggers dynamic recrystallization during subsequent mushy state rolling. It should also be noted that grain size reduction is continued, but is less significant on subjecting to multiple roll passes in mushy state. The cause of third observation is the use of a constant rolling speed, which leads to the same cooling rate for multiple mushy state roll passes. As a result, the average size of finer grains obtained by rapid solidification of liquid appears not to change much. However, the unmelted solid skeleton undergoes repeated fragmentation and dynamic recrystallization, leading to the reduction in average grain size.

Table 1
The average sizes of coarse and fine grains in the investigated materials.

Material	Average grain size (μm)	
	Coarse	Fine
MRA	351 ± 218	194 ± 96
HRC	52 ± 15	32 ± 10
MRC	51 ± 11	31 ± 12
PHMPR1	42 ± 09	29 ± 10
PHMPR2	39 ± 12	28 ± 09
PHMPR3	35 ± 10	26 ± 10

A combination of SEM image and EDS X-ray maps of Ti and Cu has been shown for ACC, MRC and PHMPR2 in Figs. 2–4, respectively. Examination of the SEM image [Fig. 2(a)] and the EDS X-ray map of Ti [Fig. 2(b)] obtained from the sample of ACC indicate that the TiB_2 particles are present in the form of a network at

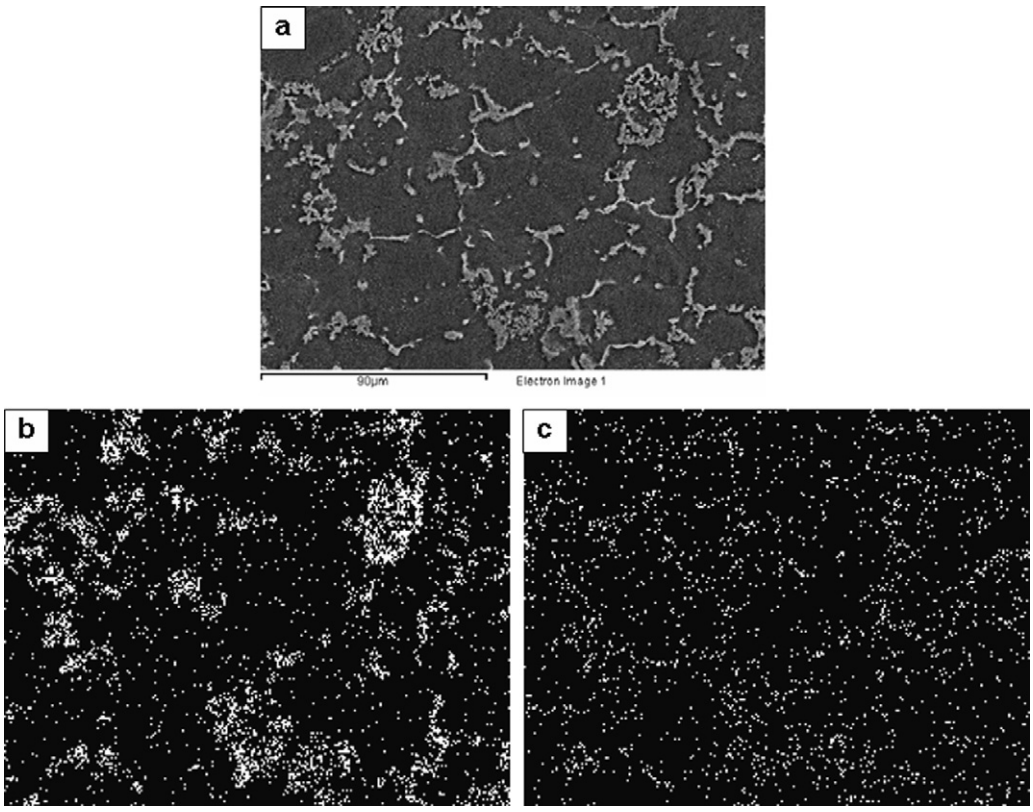

Fig. 2. (a) SEM (SE) image depicting microstructure of ACC, and EDS X-ray maps of: (b) Ti, and (c) Cu.

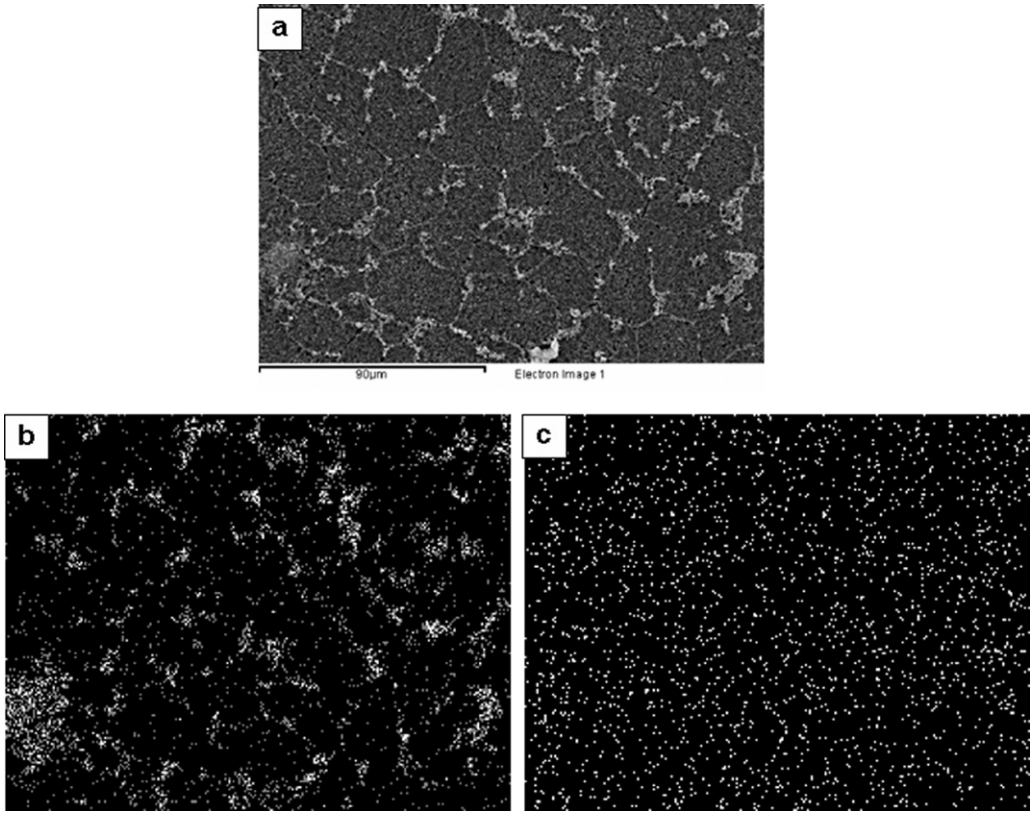

Fig. 3. (a) SEM (SE) image depicting microstructure of MRC, and EDS X-ray maps of: (b) Ti, and (c) Cu.

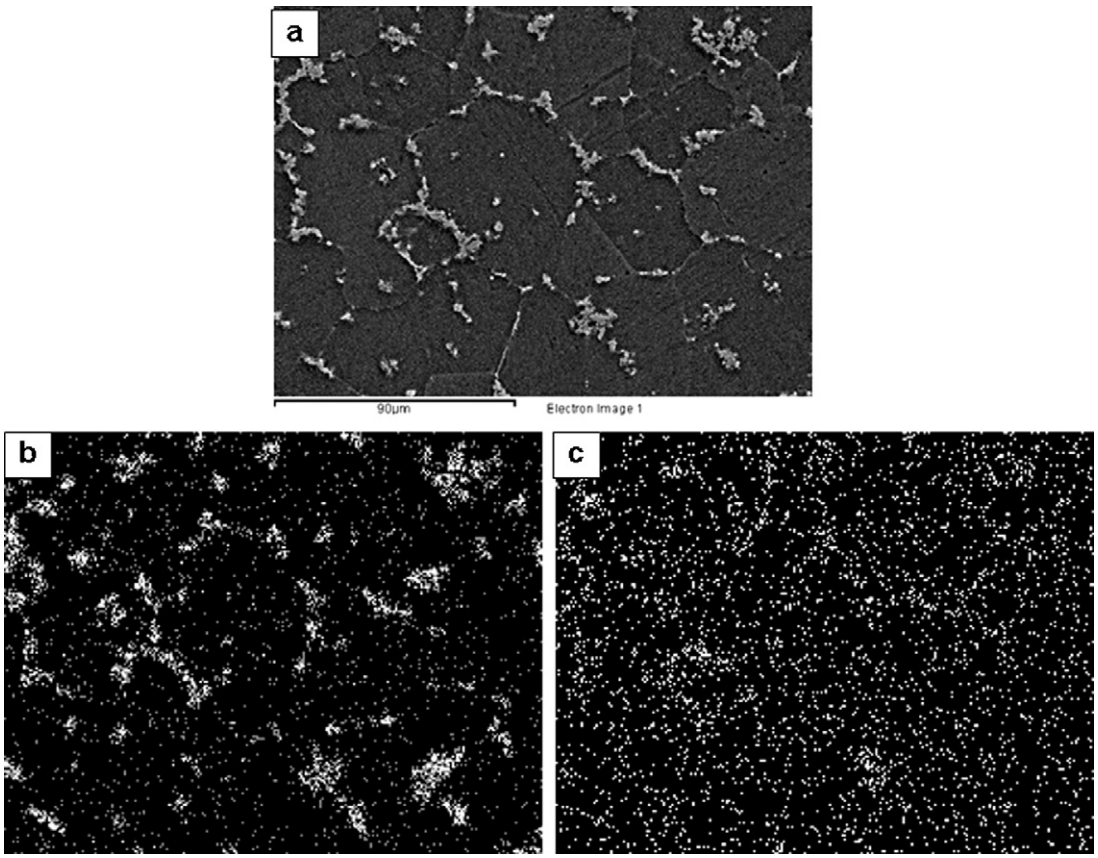

Fig. 4. (a) SEM (SE) image depicting microstructure of PHMPR2, and EDS X-ray maps of: (b) Ti, and (c) Cu.

the α-Al grain boundaries. However, examination of SEM images depicting microstructures [Figs. 3(a) and 4(a)] as well as Ti maps [Figs. 3(b) and 4(b)] of the mushy state rolled composites confirms significant redistribution of TiB_2 particles with disruptions of their grain boundary based networks. Moreover, the EDS X-ray maps in Figs. 3(c) and 4(c) indicate that distribution of Cu is more homogeneous in MRC and PHMPR1 than that in the ACC.

3.1.2. Solutionized and aged condition

Examination of the microstructure of solutionized ACA [Fig. 5(a)] and corresponding EDS X-ray map of Cu [Fig. 5(b)] as well as that from MRA [Fig. 5(c) and (d)] shows the presence of α-Al–$CuAl_2$ eutectic at intergranular locations. Formation of eutectic at grain boundaries or within the grains of MRA as reported by Herbert et al. [24,26] has been attributed to localized enrichment of Cu in liquid Al during soaking at the mushy zone temperature. This liquid is trapped either at the grain boundaries or inside the grains of α-Al, and undergoes rapid solidification in course of passage through the roll gap. Hence, the average Cu concentration of the matrix is reduced as a result of the presence of Cu-rich eutectic in ACA or MRA. Evidence for segregation of Cu has also been found at grain boundaries of solutionized ACC, as is obvious on examination of the SEM (BSE) image and EDS X-ray map of Cu, shown in Fig. 6(a) and (b), respectively. However, the distribution of Cu has been found to be relatively more uniform in the microstructure of MRC, as shown in SEM (BSE) image [Fig. 6(c)] and EDS X-ray map [Fig. 6(d)].

Fig. 7 shows the XRD pattern obtained from the PHMPR3 specimen in peak-aged condition. The peaks of $CuAl_2$ in the XRD pattern confirm the formation of precipitates in the Al alloy matrix. The distribution of $CuAl_2$ precipitates in ACA, MRA, ACC, MRC, PHMPR1 and PHMPR2 in their peak-aged condition is shown qualitatively using EDS X-ray maps depicting enrichment of Cu in Fig. 8(a)–(f), respectively. Comparison of these figures suggests that distribution of Cu is more uniform in the MRA than that in the ACA. Similarly, the distribution of Cu in the composite matrices appears to improve in the following order: ACC < MRC < PHMPR1. The distributions of Cu in the matrices of peak-aged PHMPR1 and PHMPR2 appear to be more or less similar. Thus, the uniformity in distribution of precipitates appears to be the worst in case of ACA or ACC, and the most impressive in case of PHMPR1 or PHMPR2. Comparison of the results in Fig. 8 with that shown in Figs. 2–6 indicate that the trend followed in distribution of $CuAl_2$ precipitates is closely related to the amount of uniformity of Cu atom distribution in the matrix prior to aging. Moreover, greater uniformity in the distribution of precipitates in PHMPR1 than that observed in the microstructure of MRC indicates that prior hot rolling has a significant effect on homogenization of Cu atom distribution in the matrix.

Typical bright field TEM images from the peak-aged ACA and PHMPR3 specimens are shown in Fig. 9(a) and (b), respectively. Examination of these figures leads to following inferences: (i) $CuAl_2$ precipitates with sizes ranging between 10 and 20 nm are formed on the dislocation lines; (ii) the region of matrix around a TiB_2 particle has a high density of dislocation tangles along with precipitates; (iii) the density of precipitates appears to be lower, and their distribution is more uniform in the matrix of the composite than that in the alloy.

3.2. Aging kinetics using micro-hardness measurements

Fig. 10(a) presents plots showing the variation of matrix microhardness with time of aging for the investigated alloy and composite in as cast, hot rolled or mushy state rolled conditions. Microhardness of all the samples in solutionized condition is

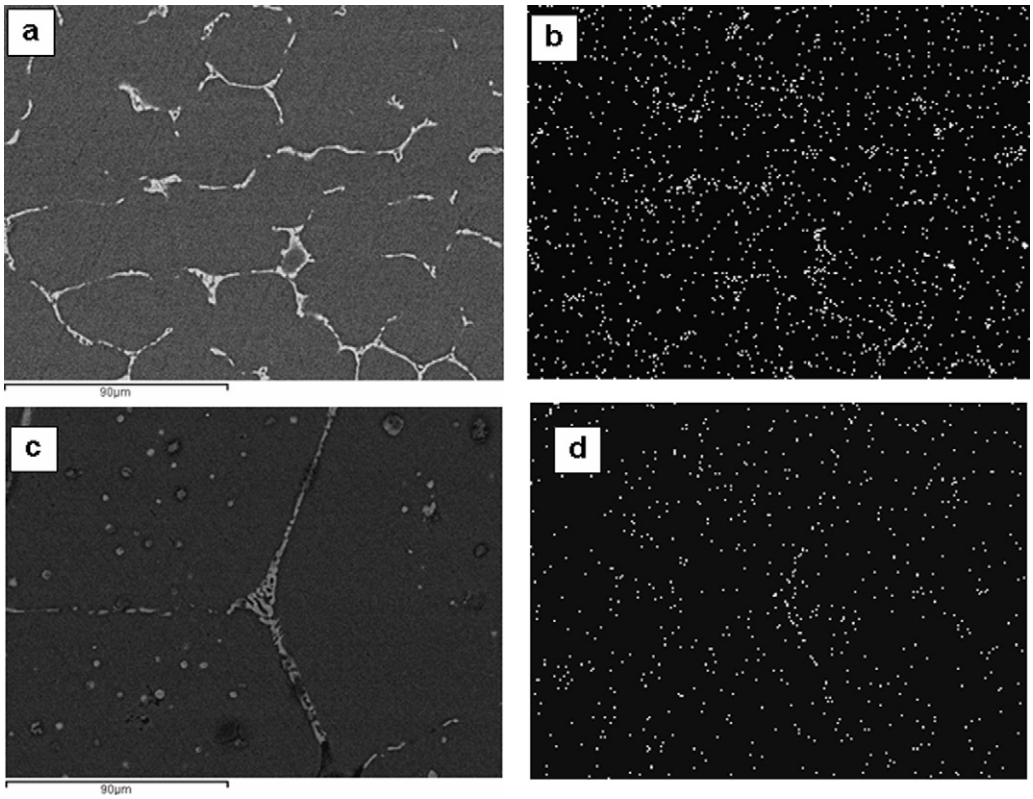

Fig. 5. (a) SEM (BSE) image and (b) EDS X-ray map of Cu in solutionized ACA; as well as (c) SEM (BSE) image and (d) EDS X-ray map of Cu in solutionized MRA.

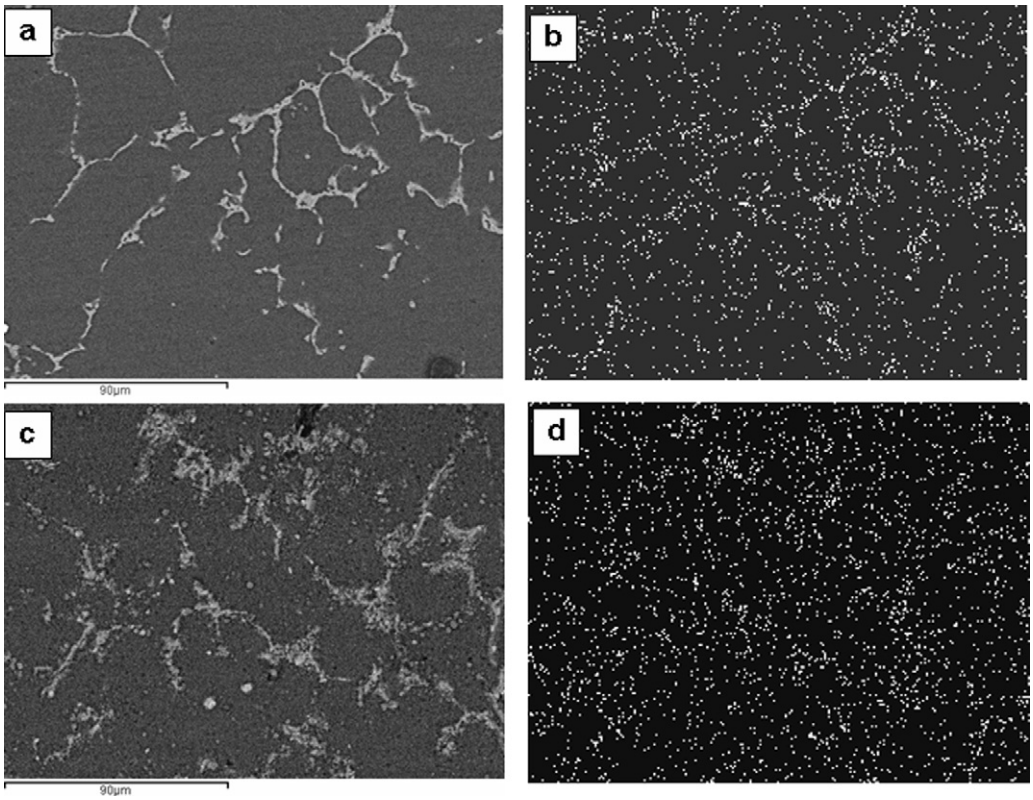

Fig. 6. (a) SEM (BSE) image and (b) EDS X-ray map of Cu in solutionized ACC; as well as (c) SEM (BSE) image and (d) EDS X-ray map of Cu in solutionized MRC.

represented by the data point corresponding to 0 h. Examination of the results in this figure leads to the following inferences: (i) the composite in as-cast and mushy state rolled condition takes only 60% and 10%, respectively of the total time (20 h) taken by the ACA to reach the peak-age condition; while (ii) the peak-age microhardness observed for the ACC and MRC is higher than that of ACA by 26% and 39%, respectively. Furthermore, examination of the plots in Fig. 10(b) indicates that the aging time is further reduced to 1.5 h for the composites subjected to multiple roll passes in mushy state (PHMPR2 and PHMPR3). The peak-age microhardness increases in following the order: MRA < ACA < ACC < HRC < MRC < PHMPR1 < PHMPR2 < PHMPR3, with the highest value of 126 H_V being recorded for the PHMPR3. The time for peak-aging has been found to decrease in the same order, except for the fact that the matrix in ACA takes 67% more time to reach the maximum microhardness than that of MRA (12 h). The lower peak-age microhardness of the MRA than that of ACA may be attributed to the coarser average grain size in the former material, as is obvious from the results shown in Fig. 1 and Table 1.

The aging kinetics has been quantified in terms of the rate of age hardening of the composite (R), which is defined as follows:

$$R = \frac{\text{peak-age microhardness} - \text{microhardness in solutionized condition}}{\text{peak-aging time}} \quad (1)$$

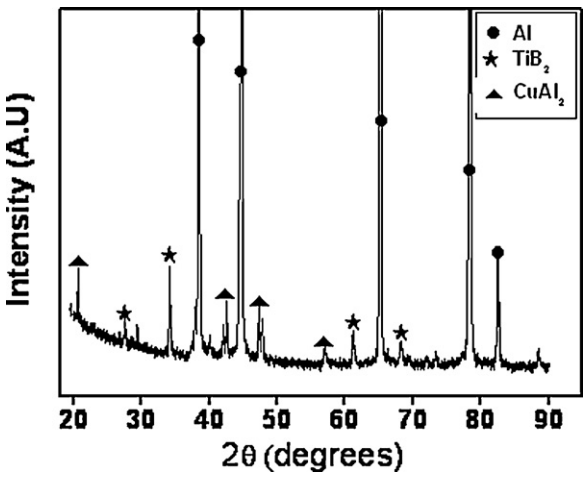

Fig. 7. XRD pattern from the peak-aged PHMPR3 showing the peaks of Al, TiB_2 and $CuAl_2$ phases.

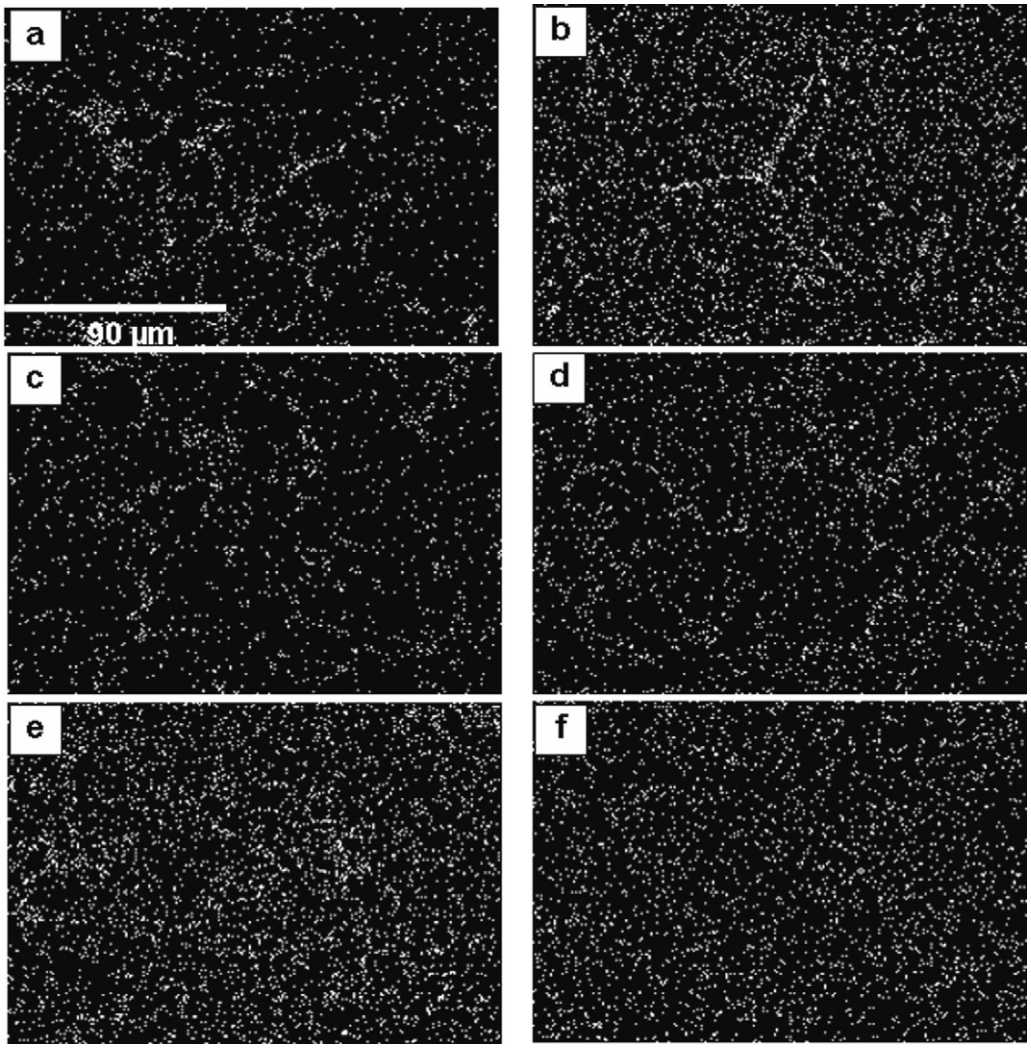

Fig. 8. EDS X-ray maps depicting enrichment pattern of Cu in the microstructures of: (a) ACA, (b) MRA, (c) ACC, (d) MRC, (e) PHMPR1, and (f) PHMPR2.

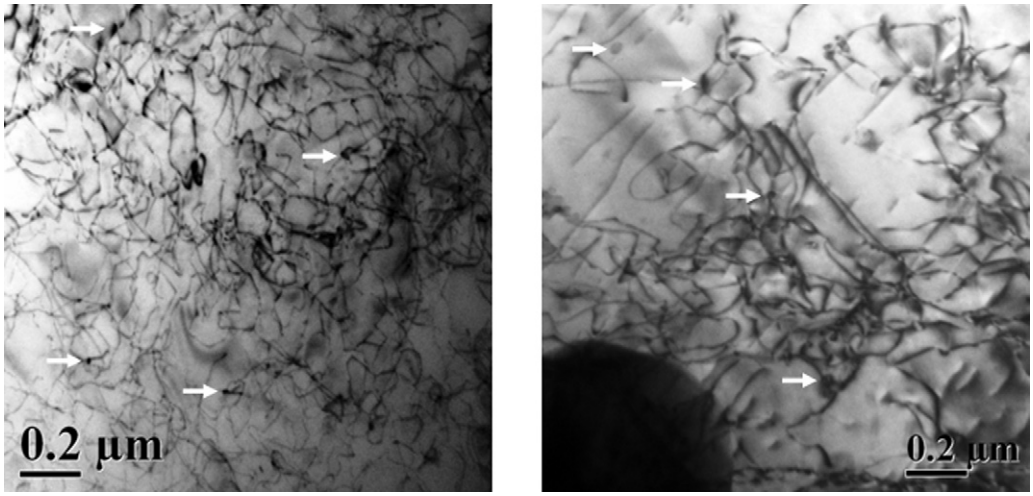

Fig. 9. Bright field TEM image from peak-aged specimens of: (a) ACC, and (b) PHMPR3. Typical $CuAl_2$ precipitates attached to dislocations are marked with arrows.

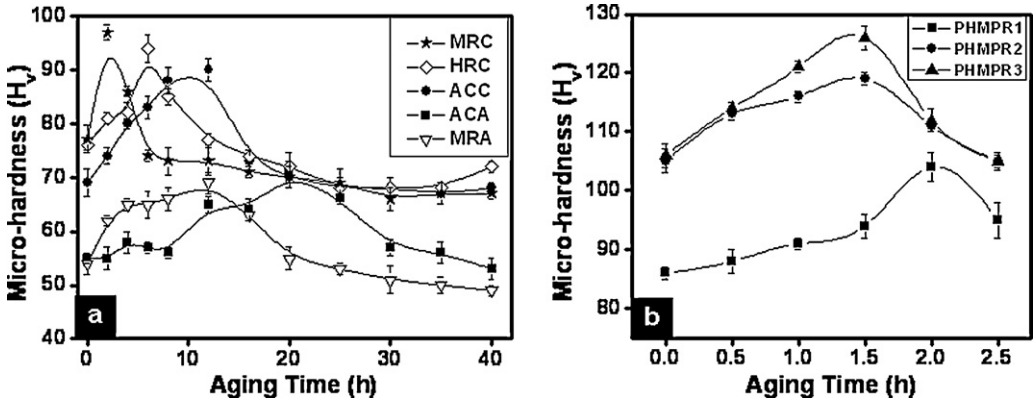

Fig. 10. Plots showing the variation of microhardness with time of aging for: (a) alloy and composite samples in as-cast, hot rolled or mushy state rolled conditions; (b) composite samples subjected to single or multiple mushy state roll passes after prior hot rolling.

The values of *R* for both alloy and composite in either as-cast or mushy state rolled conditions are presented using bar charts in Fig. 11. Analysis of the results in this figure indicates that *R* increases in the order of ACA < MRA < ACC < HRC < MRC < PHMPR1 < PHMPR2 < PHMPR3. It is also interesting to note that the values of *R* are somewhat similar for MRC and PHMPR1, which confirms that mushy state rolling has a much greater effect on the precipitation kinetics than prior hot rolling of the composites.

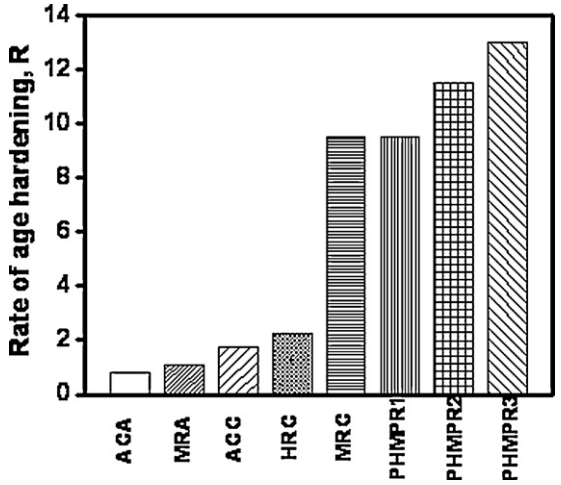

Fig. 11. Bar charts depicting the rate of age-hardening of the as-cast and mushy state rolled alloy, and the as-cast, hot, mushy state and pre-hot rolled mushy state rolled composite.

The plot A in Fig. 12 shows the difference between the microhardness obtained for the peak-aged and the corresponding solution-treated conditions of both alloy and composite in as-cast, hot rolled or mushy state rolled conditions, while the plot B depicts the microhardness increment of the peak-aged alloy or composite matrix with respect to that of the unreinforced, solution-treated alloy. On examination of these plots, it is possible to distinguish between the increments in hardness achieved due to the presence of $CuAl_2$ precipitates alone in a given material (plot A), and that due to the presence of TiB_2 particles as well as hot or mushy state rolling (plot B). While the contribution of precipitation hardening to peak age hardness appears as more or less same for both alloy and composite (plot A), that due to the presence of TiB_2 reinforcement and deformation processing are found to be more significant (plot B).

3.3. Tensile properties of ACA, ACC and MRC

Typical true stress–true strain curves of ACA, ACC and MRC samples in peak-aged condition are shown in Fig. 13(a), while those of the MRC in solutionized, under-aged, peak-aged and over-aged conditions are shown in Fig. 13(b). Examination of the results in Fig. 13(a) and (b) shows the presence of serrations in the stress–strain curves for the peak-aged ACA and ACC, as well as the

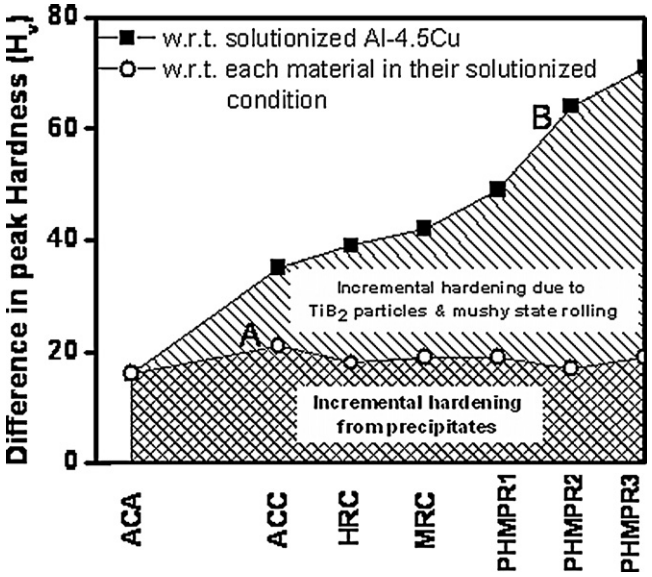

Fig. 12. Plots showing hardness increment observed in as-cast, hot and mushy state rolled composite with respect to that in: (a) its solution treated condition; and (b) as-cast, solution treated alloy.

solution-treated MRC with evidence for different amounts of strain hardening. Bar charts representing the yield and ultimate tensile strengths obtained from the engineering stress–strain curves of the ACA, ACC and MRC in peak-aged condition are shown in Fig. 14(a), while those of the MRC in solutionized, or differently aged conditions are shown in Fig. 14(b). Comparison of the bar charts in Fig. 14(a) shows that the yield and ultimate tensile strengths are almost same for ACA and ACC in their peak-aged condition, but less than that of the peak-aged MRC. For the MRC [Fig. 14(b)], both the yield and ultimate tensile strengths are found to increase with increase in the aging time, till the peak-age condition is attained and are decreased on over-aging, as expected.

Table 2
Strain-hardening exponent (n) and strength coefficient (K) of the MRC.

Condition	Strain-hardening exponent (n)	Strength coefficient (K) (MPa)
Solution-treated	0.51	2.78
Under-aged	0.56	2.89
Peak-aged	0.57	2.95
Over-aged	0.56	2.87

Bar charts depicting uniform elongation (e_u) and elongation to failure (e_f) for the ACA, ACC and MRC in peak-aged condition are shown in Fig. 15(a), while those of the MRC in solutionized, and differently aged conditions are shown in Fig. 15(b). Comparison of the bar charts in Fig. 15(a) and (b) leads to the following inferences regarding e_u and e_f: (i) their values are found to be the greatest for the peak-aged ACA, and appear to be the least for the peak-aged MRC; (ii) these quantities are found to be higher for the solutionized or under-aged MRC samples than that for peak-aged or over-aged samples. Study of fracture surfaces has shown the presence of dimples as evidence for ductile failure.

Table 2 presents the values of strain hardening exponent (n) and strength coefficient (K) for the MRC subjected to different aging heat-treatments. Furthermore, the rates of strain hardening

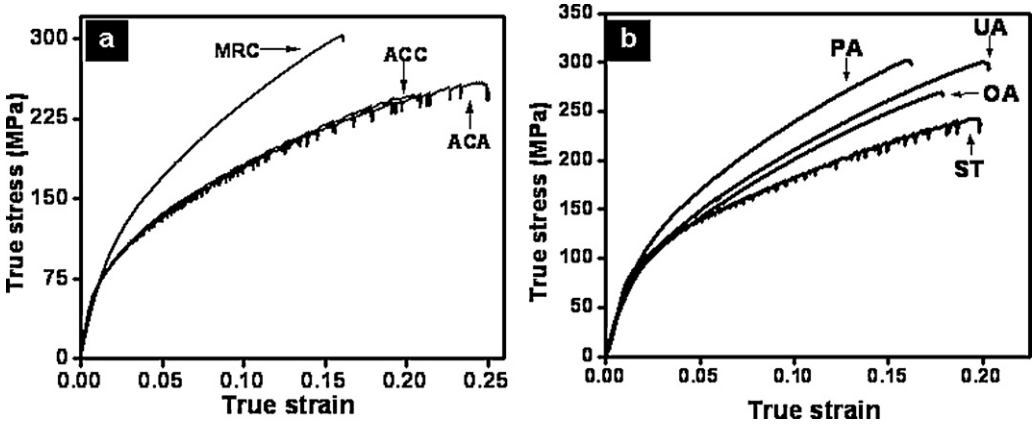

Fig. 13. Plots showing the typical stress–strain curves: (a) ACA, ACC and MRC in peak-aged condition; as well as of (b) MRC under differently aged conditions.

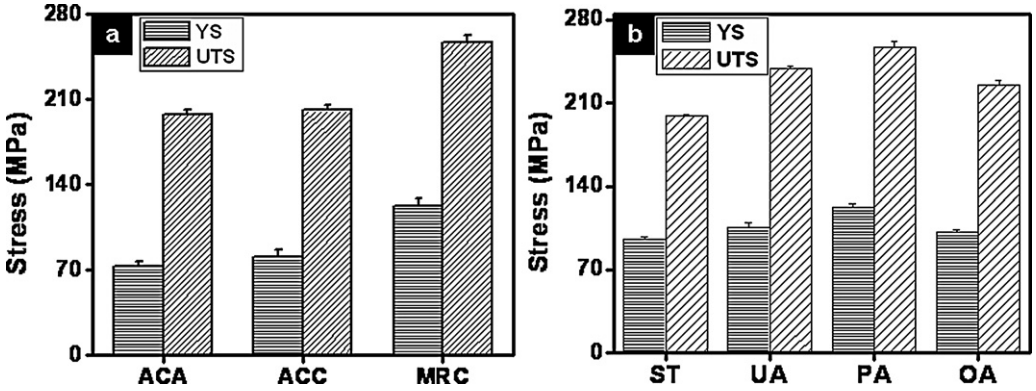

Fig. 14. Bar charts showing the room temperature yield (YS) and ultimate tensile strengths (UTS) of the: (a) ACA, ACC as well as MRC in peak-aged condition; and (b) MRC in its differently aged conditions.

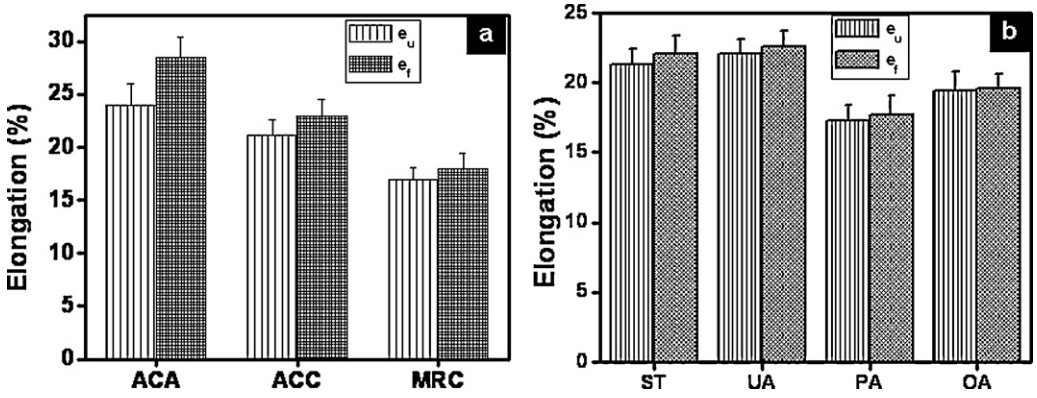

Fig. 15. Bar charts showing uniform elongation (e_u) and elongation to failure (e_f), obtained from the engineering stress–strain curves for room temperature tension tests carried out on: (a) ACA, ACC and MRC in peak-aged condition; as well as (b) MRC in solution-treated, under-aged, peak-aged and over-aged conditions.

($d\sigma/d\varepsilon_p$) obtained by analysis of the true stress–true strain data (as shown in Fig. 13) are plotted against true plastic strain (ε_p) in Fig. 16(a) and (b). Examination of these plots leads to the following inferences about the rate of strain hardening: (i) it is higher for the peak-aged MRC than those of peak-aged ACA and ACC; and (ii) it is maximum for the MRC in peak-aged condition, followed by those for the samples in under-aged, over-aged, and solution-treated conditions.

4. Discussion

4.1. Aging kinetics

The results of this study have shown that the presence of TiB_2 particles combined with subjecting of these materials to either single or multiple mushy state roll passes, leads to significant acceleration of aging kinetics of the Al–4.5Cu alloy matrix. Results of the present study pertaining to the effect of TiB_2 reinforcement are in agreement with that reported in the literature [8–10] about the aging kinetics of age-hardenable Al alloy-based composites. Moreover, enhancement in the aging kinetics of the Al–Cu alloy matrix of the composite due to the presence of TiB_2 reinforcement has also been reported earlier [9,11]. The precipitation kinetics of the matrix in these composites has been reported to be significantly enhanced, primarily due to the higher density of dislocations than that in the corresponding monolithic alloys. The dislocations are known to be energetically favorable sites for nucleation of the $CuAl_2$ precipitates, as is obvious from the results of TEM studies (Fig. 9). Furthermore, the dislocation cores allow short circuit paths for pipe diffusion of solute atoms in the matrix of the composites, which decreases the incubation period for formation of precipitates and aid in their growth. The dislocation density is expected to be higher in the composites due to: (i) strain caused by thermal expansion mismatch between reinforcement and matrix during quenching after solution treatment, and (ii) grain refinement. Moreover, redistribution of the TiB_2 particles is expected to have a significant effect on the dislocation density throughout the matrix.

The strain, ε created at a given particle–matrix interface on quenching due to the difference in the values of coefficients of thermal expansion (CTE) of Al (23.5×10^{-6}/K) and TiB_2 (7×10^{-6}/K) [29], is given by the following relationship:

$$\varepsilon = \Delta T \times \Delta \mathrm{CTE} \tag{2}$$

In the present study, the strain due to CTE mismatch is calculated as 12.67×10^{-3}. The density of dislocations with the Burgers vector, b, generated as a result of quenching from 495 °C to 0 °C (ice-cold water) has been calculated using the following equation [18]:

$$\rho = \frac{BV_f\varepsilon}{bt(1 - V_f)} \tag{3}$$

where 'B' is a constant having value between 4 and 12, 'V_f' is the volume fraction, and 't' is the smallest dimension of the reinforcement. Considering $V_f = 0.031$, $b = a/2[1\,1\,0] = 0.286$ nm, $t = 1.5$ μm, ρ due to CTE mismatch has been found to be 9.5×10^8 B m/m^3.

The increase in dislocation density due to ΔCTE alone cannot be considered as solely responsible for enhancement in aging kinetics, particularly because the effect of mushy state rolling and multiple mushy state roll passes appears more significant, as is obvious from the results presented in Fig. 12. The contribution of grain refinement and particle redistribution (as shown in Figs. 2–4) with

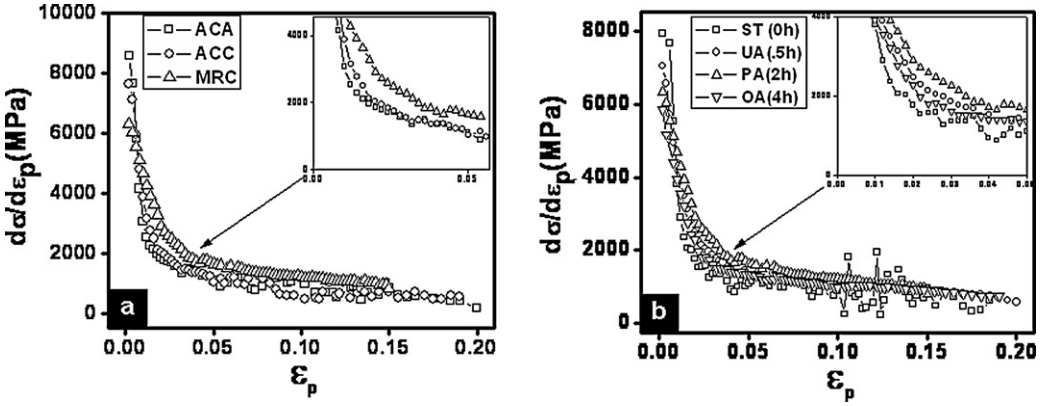

Fig. 16. Plots showing the variation of rate of strain hardening ($d\sigma/d\varepsilon_p$) with true plastic strain (ε_p) for tension tests carried out on the: (a) ACA, ACC and MRC in peak-aged condition; (b) MRC in differently aged conditions. A magnified view of a section of the plots is shown as an inset to make the difference more obvious.

increase in the number of mushy state roll passes also appears to have significant role in uniformly increasing dislocation density throughout the matrix. Moreover, greater uniformity in Cu atom distribution (Figs. 2–4) achieved by mushy state rolling is expected to increase the density of precipitates and lead to a more uniform distribution, as inferred by examining the results depicted in both the EDS X-ray maps of Cu (Fig. 8) and the TEM images (Fig. 9). In an earlier study [30], it has been shown that segregation of Cu to particle–matrix interfaces in composites or its presence in the form of intermetallics leads to a lower Cu concentration in the solution-treated alloy matrix. Reduction in the concentration of Cu in the alloy matrix is believed to reduce the chemical driving force for precipitation, which in turn has been found to cause slow-down in the kinetics of aging in the matrix of the composite with respect to that in the monolithic alloy. Hence, reduction in the amount of Cu segregation at grain boundaries or inter-dendritic locations, and its re-distribution can be considered to play a major role in enhancement of aging kinetics of the Al alloy matrix in the investigated mushy state rolled composites.

4.2. Strengthening mechanisms

Observations of TEM images in Fig. 9(a) and (b) have revealed the existence of strong interactions of dislocations with precipitates in the matrix. The precipitates are able to pin the dislocations, and thus hinder their movement, which in turn leads to a significant amount of strengthening in the investigated materials. It is intuitive that with increase in density of precipitates and uniformity in their distribution, the inter-particle spacing is reduced and hindrance to dislocation motion is increased. Although both MRC and PHMPR1 show similar aging kinetics, the peak-age microhardness of the latter material is higher by 10.8%, which can be attributed to smaller matrix grain size (Table 1) as well as greater uniformity of precipitate distribution in its microstructure, as is evident on comparing the EDS X-ray maps of Cu in Fig. 8(d) and (e).

4.3. Tensile behavior

The tensile properties obtained for ACA and ACC in this study have been found to be comparable to the values reported in the literature [31,32] for as-cast or rheocast Al–Cu alloys. Comparative investigation of the tensile properties of the peak-aged materials has shown the results to be in agreement with the trends found for hardness. Thus, the MRC has shown significantly higher yield and ultimate tensile strengths as well as rate of strain hardening compared to those of the ACC. These results may be attributed to higher nucleation density of precipitates with smaller inter-particle spacing, causing greater obstacle for the motion of dislocations. However, the increase in strength (Fig. 14) and strain hardening ability (Fig. 16) of the peak-aged MRC is found to be at the expense of tensile ductility (Fig. 15), which may be attributed to restrictions to dislocation mobility on account of much shorter inter-particle spacing in this material.

The serrations observed in the flow curves shown in Fig. 13(a) and (b) are consistent with that reported in earlier studies [33,34], and are attributed to dislocation–solute atom interactions, rather than shearing of coherent precipitates by dislocations. This argument follows from the observation that the stress–strain curves of only the solution-treated MRC show serrations [Fig. 13(b)], while those representing under-aged or over-aged conditions of the matrices do not show such features. A study by Chmelik et al. [35] has shown no evidence to suggest the shearing of precipitates as responsible for serrations in the plastic flow curve. In fact, the serrations were found to be suppressed on precipitation in peak-aged Al–Zn and Al–Li alloys, similar to the observations recorded for the MRC. Thus, the presence of serrations in stress–strain curves of peak-aged ACA and ACC may be attributed to incomplete precipitation, probably due to dendritic segregation of Cu.

5. Conclusions

The isothermal aging kinetics of as-cast and mushy state rolled Al–4.5Cu alloy and in situ Al–4.5Cu–5TiB_2 composite subjected to mushy state rolling has been studied. The following conclusions can be drawn from the present study.

Addition of 5 wt.% TiB_2 reinforcements to the Al–4.5Cu alloy increases the peak-age microhardness of the matrix by ≈30%, while reducing the time required to reach it by ≈40%. The time required for peak-aging is reduced for both alloy and composite on mushy state rolling, with the enhancement in aging kinetics being more significant for the latter material. The time for peak-aging and peak-age microhardness of the PHMPR3 has been found as ≈12.5% and ≈144%, respectively of that found for the ACC. The peak-age microhardness increases in the order of MRA < ACA < ACC < HRC < MRC < PHMPR1 < PHMPR2 < PHMPR3. On the other hand, the time for peak aging decreases in the same order, except for the fact that the positions of ACA and MRA are exchanged.

Examination of the microstructures using TEM has shown the presence of $CuAl_2$ precipitates having sizes mostly in the range of 10–20 nm, majority of which appear to nucleate at dislocations. In addition to the increase in dislocation density in the alloy matrix due to coefficient of thermal expansion mismatch between matrix and reinforcement, grain refinement and redistribution of TiB_2 particles, greater uniformity in Cu atom distribution in the matrix appears to have a significant role in enhancing aging kinetics, uniformity in distribution of $CuAl_2$ precipitates, as well in increasing the strength achieved by age-hardening. Strong interaction between dislocations and precipitates has been found to be the predominant strengthening mechanism.

The YS, UTS and strain hardening rates of the mushy state rolled composite in peak-aged condition are found to be significantly greater than those of peak-aged as-cast alloy and composites specimens. For the mushy state rolled composite, YS and UTS have been found to be the highest for peak-aged condition, while maximum elongation has been recorded for under-aged condition.

This study has shown that mushy state rolling with prior hot rolling is an attractive deformation processing step for the as-cast composites, because it leads not only to enhancement of the aging kinetics, but also to a sharp increase in the strength achieved in peak-aged condition.

Acknowledgements

The authors wish to thank Mr. K. Saw and P. Das, Department of Metallurgical and Materials Engineering, IIT Kharagpur for the valuable technical assistance provided during processing of the material. The assistance rendered by Mr. S. Mondal and Mr. Mithun Das with SEM and Mr. Ranadhir Bose with TEM studies at the Central Research Facility, IIT Kharagpur are gratefully acknowledged.

References

[1] J.E. Allison, G.S. Cole, J. Met. 45 (1) (1993) 19–24.
[2] G. Hirt, R. Cremer, T. Witulski, H.C. Tinius, Mater. Des. 18 (4/6) (1997) 315–321.
[3] D.B. Miracle, Comp. Sci. Technol. 65 (2005) 2526–2540.
[4] T.G. Neih, R.F. Karlak, Scripta Metall. 18 (1) (1984) 25–28.
[5] J.M. Papazian, Metall. Trans. A 19 (1988) 2945–2953.
[6] P. Appendino, C. Badini, F. Marino, A. Tomasi, Mater. Sci. Eng. A 135 (1991) 275–279.
[7] J.S. Lin, P.X. Li, R. Wu, Scripta Metall. Mater. 28 (1993) 281–286.
[8] C. Bartels, D. Raabe, G. Gottstein, U. Huber, Mater. Sci. Eng. A 237 (1997) 12–23.
[9] A. Mandal, R. Maiti, M. Chakraborty, B.S. Murty, Mater. Sci. Eng. A 386 (2004) 296–300.
[10] A. Mandal, M. Chakraborty, B.S. Murty, Mater. Sci. Eng. A 489 (2008) 220–226.

[11] S. Kumar, V. Subramanya Sarma, B.S. Murty, J. Alloys Compd. 479 (2009) 268–273.
[12] T. Christman, S. Suresh, Acta Metall. 36 (7) (1988) 1691–1704.
[13] K.K. Chawla, A.H. Esmaeli, A.K. Datye, A.K. Vasudevan, Scripta Metall. Mater. 25 (6) (1991) 1315–1319.
[14] I. Dutta, S.M. Allen, J.L. Hafley, Metall. Trans. A 22 (1992) 2553–2563.
[15] M.P. Thomas, J.E. King, J. Mater. Sci. 29 (1994) 5272–5278.
[16] V.K. Varma, Y.R. Mahajan, V.V. Kutumba Rao, Scripta Metall. 37 (4) (1997) 485–489.
[17] K.K. Chawla, M. Metzer, J. Mater. Sci. 7 (1972) 34–39.
[18] R.J. Arsenault, N. Shi, Mater. Sci. Eng. A 81 (1986) 175–187.
[19] M.M. Rovira, B.C. Lancini, M.H. Robert, J. Mater. Proc. Technol. 92–93 (1999) 42–49.
[20] L. Zu, S. Luo, J. Mater. Proc. Technol. 114 (3) (2001) 189–193.
[21] M. Kiuchi, S. Sugiyama, K. Arai, J. Jpn. Soc. Technol. Plast. 20 (223) (1979) 762–765.
[22] A. Tseng, J. Horsky, M. Raudensky, P. Kotrbacek, Mater. Des. 22 (2) (2001) 83–91.
[23] H.V. Atkinson, K.J. Burke, G. Vaneetveld, Mater. Sci. Eng. A 490 (2008) 266–276.
[24] M.A. Herbert, C. Sarkar, R. Mitra, M. Chakraborty, Metall. Trans. A 38 (2007) 2110–2126.
[25] M.A. Herbert, R. Maiti, R. Mitra, M. Chakraborty, Wear 265 (2008) 1606–1618.
[26] M.A. Herbert, G. Das, R. Maiti, M. Chakraborty, R. Mitra, Inter. J. Cast Metal. Res. 23 (4) (2010) 216–224.
[27] E. Tzimas, A. Zavaliangos, J. Mater. Sci. 35 (2000) 5319–5329.
[28] ASM Handbook, Heat Treating, vol. 4, ASM International, Materials Park, OH, USA, 1997, pp. 841–887.
[29] S.K. Varma, J. Ponce, M. Solis, S. Andrews, D. Salas, Metall. Trans. A 27 (1996) 2023–2203.
[30] Sharmilee Pal, R. Mitra, V.V. Bhanuprasad, Mater. Sci. Eng. A 480 (1–2) (2008) 496–505.
[31] S. Skolianos, Mater. Sci. Eng. A 210 (1996) 76–82.
[32] E.J. Zoqui, M.H. Robert, J. Mater. Proc. Technol. 78 (1998) 198–203.
[33] A. Rosen, Mater. Sci. Eng. A 7 (4) (1971) 191–202.
[34] A. Wijler, M.M.A. Vrijhoef, A. Van Den Beukel, Acta Metall. 22 (1974) 13–19.
[35] F. Chmelik, E. Pink, J. Król, J. Balik, J. Pešička, P. Lukáč, Acta Mater. 46 (1998) 4435–4442.